sciendo Applied Mathematics and Nonlinear Sciences, 9(1) (2024) 1-17

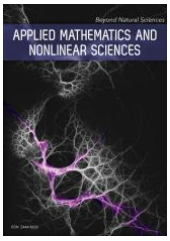

Applied Mathematics and Nonlinear Sciences

https://www.sciendo.com

Real-time tracking of the effect of jumping rope exercise using a wearable device

Diyang Liu[1,†], Qiang Zhang[1]

1. Fuyang Normal University, Fuyang, Anhui, 23600, China.

Submission Info

Communicated by Z. Sabir
Received March 1, 2024
Accepted May 20, 2024
Available online July 5, 2024

Abstract

With the development of science and technology, wearable devices, as an emerging field, have been gradually integrated into our daily lives and are widely used in the tracking of movement effects. In this paper, the data fusion algorithm combining complementary filtering and extended Kalman filtering and the human posture solving algorithm based on the D-H method is selected to solve the designed human jumping rope motion joint model, which realizes the construction of a wearable jumping rope motion capture system. Furthermore, the effect and commercial value of the wearable device designed in this paper for real-time tracking of jumping rope movement are tested by a single node posture test and a comparison experiment with posture solving. The experimental results show that the static test error and dynamic test accuracy of the sensor are 1.4° and 4°, respectively, which indicate that the sensor can accurately recognize the trajectory of jumping rope movements. The average values of RMSE for pitch angle, roll angle, and yaw angle were 0.37, 0.69, and 1.40, respectively. This indicates that the wearable device and the pose-solving algorithm used in this paper can meet the standard for commercial applications. This study provides a new approach to studying sports, which has rarely been done in the field of smart sports.

Keywords: Wearable devices; Motion capture; Jump rope sport; Human posture solving; Data fusion.
AMS 2010 codes: 68P30

†Corresponding author.
Email address: ldy19902024@163.com

ISSN 2444-8656
https://doi.org/10.2478/amns-2024-1601

1 Introduction

The rapid development of the information age has brought a lot of convenience to people's lives, and at the same time, it has a great impact on the traditional industry [1]. The conventional way of exercise can not satisfy people's desire for training, intelligence, data, accuracy has been gradually emphasized by people [2]. Wearable devices came into being. Wearable devices are sensors combined with cell phone application apps that record and analyze the user's behavior, location, and changes in physical and physiological indicators at any time, which can be combined with individual differences to provide appropriate exercise recommendations [3].

In the traditional classroom teaching of rope skipping, the teacher mostly explains and demonstrates, the teaching method is single, the process is boring, and the students can only learn by understanding and imitating the technical movements [4]. The application of intelligent wearable devices, the 3D simulation function, not only adds interest to the classroom but also promotes the students' learning of technical movements from a third-person perspective. In addition to the objective feedback of teaching data, but also provides teachers with new teaching ideas and methods [5-6]. The application of wearable devices will bring new development opportunities and challenges to jump rope teaching.

The smart rope-skipping evaluation system is designed and developed with a computer and the Internet as the carrier, using sensors to collect human data in real-time. After processing, it is transmitted to the server, which analyzes and processes the data to get the corresponding conclusions. Finally, it forms a complete evaluation system, which makes it easy for teachers to understand the training situation of the students in a timely manner and to formulate more suitable training methods for the students at different levels [7-8]. Not only can students better understand their physical fitness, but also provide teachers with appropriate guidance. It helps to enhance students' interest in learning and inspires students to actively participate in physical exercise with enthusiasm and motivation [9].

The digital and modern development of jump rope physical exercise and teaching in colleges and universities will certainly lead to the expansion and updating of the specific content of teaching, and teachers can take the semester as a teaching cycle to develop a new teaching model that is different from the existing exercise content. Guo, W. verified through the example of jump rope exercise that aerobic exercise promotes the improvement of brain function and enhances the brain's ability to learn and the coordination characteristics of limb control [10]. Ha, A. S. et al. observed 176 girls jumping rope for two school years and found that jumping rope promoted bone mineral density in girls [11]. David Hortigüela Alcalá et al. concluded, based on questionnaire data from a jump rope teaching experiment, that differences in motivation affect the level of effort in physical education learning, as well as the amount of time willing to spend [12]. Johnston, W. et al. reviewed the related literature and tried to design a step counter verification protocol for wearables and smartphones to improve the functionality and convenience of wearables [13]. Huang, Y. et al. conceived a wearable behavior recognition system with an integrated energy utilization model and a multi-objective particle swarm optimization algorithm as the underlying architecture to balance energy saving, user satisfaction, and functionality [14]. Sattler, M. C et al. discussed the testing credibility of wearable devices. They concluded that wearable devices are professionally identified as advanced instruments, and the measurements they provide are authentic and reliable [15]. Dargazany, A. R. et al. summarized the current status of research development and future trends in the incorporation of deep learning algorithms in wearable devices, which provides an important reference for cloud data research and intelligence research in wearable devices [16]. Wang, Y et al. drew on the Internet of Things (IoT) technology to explore the development and research and development of digital fitness equipment, aiming to provide users with professional, intelligent, and safe fitness equipment which can satisfy users' fitness needs and at the same time allow users to keep track of their own physical condition and exercise status [17].

In this study, the algorithm that combines complementary filtering and extended Kalman filtering is chosen to incorporate jumping rope exercise data. The human posture-solving algorithm based on the D-H method is used to solve the jumping rope movement posture on the fused data. The joint model of jumping rope movement is solved, and a method for tracking the effect of jumping rope movement using wearable devices is explored. A wearable jumping rope motion capture system was built, and experiments were conducted from two perspectives, single-node posture, and posture-solving comparison, to examine the reliability of the designed jumping rope motion effect tracking method. The wearable device sensors and pose-solving algorithms used are analyzed from two perspectives, static and dynamic, respectively, during the single-node pose test so as to provide a reference for real-time tracking of movement effects using wearable devices.

2 Wearable device-based motion capture model for jumping rope

2.1 Human pose solution based on the D-H method

The D-H (Denavit-Hartenberg) method is a method for kinematic modeling of robotic arms, which is mainly used for describing the kinematic properties of robotic arms and solving kinematic problems of robotic arms. In this paper, the D-H method is used to solve the collected data of human jump rope movements and to simulate the motion. First, the position and orientation of each joint in the human motion model, as well as the parent-child relationship between each linkage, are determined. The transformation matrices that contain the relative position and orientation information between each joint are calculated after that. The actual coordinates of the determined joints are obtained by multiplying the transformation matrices of every joint, and the kinematic model is obtained and solved to determine the actual motion attitude. Finally, the kinematic characteristics of each joint at different positions are derived through model solving to simulate jumping rope movement.

In this paper, the wearable device collects human jump rope data using the quaternion type data type. Quaternion is a quaternion that represents the real and imaginary parts of the three-dimensional vector and real numbers, respectively. Its advantage over other mathematical tools, such as matrices and Euler angles, is that the result is a complex result, which allows for the direct representation of rotations in three-dimensional space without the need for multi-step operations.

The quaternion representation is as follows:

$$q = w + xi + yj + zk \tag{1}$$

Where w, x, y, z are real numbers and i, j, k are imaginary units. In the quaternion, w represents the real part of the rotation and x, y and z represent the direction of the rotation axis. The quaternion can also be expressed by equation (2):

$$q = \cos\frac{\theta}{2} + \sin\frac{\theta}{2}\left(xi + yj + zk\right) \tag{2}$$

Where θ is the rotation angle and $\left(x, y, z\right)$ is the direction vector of the rotation axis. The position is solved by the D-H method, O_{XYZ} is the reference coordinate system Q_{UVW} is the follower coordinate system, and the follower coordinates system Q_{UVW} moves according to the motion of the reference coordinate system O_{XYZ}. Assuming that a point P in space is fixed in the follower

coordinate system, the coordinates of the end under the reference and follower coordinate systems are shown in equation (3):

$$P_{xyz} = \left[p_x, p_y, p_z \right]^T, P_{uw} = \left[p_u, p_v, p_w \right]^T \tag{3}$$

The point is expressed in quadratic form as:

$$P_o = 0 + p_x i + p_y j + p_z k \tag{4}$$

$$P_Q = 0 + p_u i + p_v j + p_w k \tag{5}$$

P_o is the vector representation of point P in the reference coordinate system and P_Q is the vector representation of point P in the follower coordinate system. When the follower coordinate system is rotated along either axis, the two coordinates are converted as shown in equation (6):

$$P_o = Q^{-1} \otimes P_Q \otimes Q \tag{6}$$

It can also be expressed as:

$$P_o = RP_Q \tag{7}$$

Substituting the follower coordinate system expressed as $Q = q_0 + \vec{q}$ into the above equation yields:

$$P_o = \left[\left(q_0^2 - Q^T Q \right) I + 2QQ^T - 2q_0 Q^X \right] P_Q \tag{8}$$

I is the unit matrix, Q^X is the antisymmetric matrix, and the expansion is:

$$\begin{bmatrix} p_x \\ p_y \\ p_z \end{bmatrix} = \begin{bmatrix} q_0^2 + q_1^2 - q_2^2 - q_3^2 & 2\left(q_1 q_2 - q_0 q_3\right) & 2\left(q_1 q_3 + q_0 q_2\right) \\ 2\left(q_1 q_2 + q_0 q_3\right) & q_0^2 - q_1^2 + q_2^2 - q_3^2 & 2\left(q_2 q_3 - q_0 q_1\right) \\ 2\left(q_1 q_3 - q_0 q_2\right) & 2\left(q_2 q_3 + q_0 q_1\right) & q_0^2 - q_1^2 - q_2^2 + q_3^2 \end{bmatrix} \begin{bmatrix} p_u \\ p_v \\ p_w \end{bmatrix} \tag{9}$$

Rewrite the rotation matrix as follows:

$$\begin{bmatrix} p_x \\ p_y \\ p_z \end{bmatrix} = R \begin{bmatrix} p_u \\ p_v \\ p_w \end{bmatrix} \tag{10}$$

Combining equations (9) and (10) yields the rotation matrix R:

$$R = \begin{bmatrix} q_0^2 + q_1^2 - q_2^2 - q_3^2 & 2\left(q_1 q_2 - q_0 q_3\right) & 2\left(q_1 q_3 + q_0 q_2\right) \\ 2\left(q_1 q_2 + q_0 q_3\right) & q_0^2 - q_1^2 + q_2^2 - q_3^2 & 2\left(q_2 q_3 - q_0 q_1\right) \\ 2\left(q_1 q_3 - q_0 q_2\right) & 2\left(q_2 q_3 + q_0 q_1\right) & q_0^2 - q_1^2 - q_2^2 + q_3^2 \end{bmatrix} \tag{11}$$

In describing the spatial location of specific joints, chi-square coordinates are often used, which are taken to be 4-dimensional, with the 4th component being the scale factor. If the coordinate of a point

P in space is $P=\left[p_x, p_y, p_z\right]^T$, the corresponding 4-dimensional chi-square coordinate is equivalent to $P=\left[kp_x, kp_y, kp_z, k\right]^T$, and the value of k is not unique. Usually, the value of k can be taken as 1, and the matrix form of the joint can be written as the following square matrix form:

$$T=\begin{bmatrix} R & P_T \\ 0 & 1 \end{bmatrix} \tag{12}$$

where R is the rotation matrix of the follower coordinate system along the original coordinate system, and P_T is the vector of the follower coordinate system relative to the origin of the original coordinate system.

The PN3 data transceiver is selected to be defined as the origin of the coordinate system, the hip joint is selected to be defined as the root node, the base coordinate system is regarded as rod 0, and the root node coordinate system is viewed as rod 1. The kinematic chain is established according to the human body segments. For the process of solving the collected data, the local coordinate system needs to be established first. Then, the chi-square matrix ${}^0T_i$ is constructed in accordance with the order of connection of each joint, as follows:

$${}^0T_i = {}^0T_1{}^1T_2 \cdots {}^{i-1}T_i = \begin{bmatrix} {}^\circ R_i & {}^\circ P_i \\ 0 & 1 \end{bmatrix} \tag{13}$$

Where ${}^\circ R_i$ is the rotation matrix in the i nd coordinate system and ${}^\circ P_i$ is the vector coordinate. The final calculation yields the position of joint i:

$$\overline{P_0^i} = T\overline{P_{i-1}^i} \tag{14}$$

Through the positive kinematics solution, the simulation trajectory is calculated to visualize the jumping rope movement, which provides support for the subsequent analysis of the intrinsic mechanism of human jumping rope movement.

2.2 Data fusion algorithms for wearable devices

The data fusion algorithm used in this paper is a combination of complementary filtering and extended Kalman filtering to fuse the data results measured by the sensors to obtain the required data content. The accelerometer and magnetometer are used to calculate the initial attitude angle, the gyroscope is used to construct the state equation of the system, and the Extended Kalman Filter is used to update the state equation of the system to obtain the optimal estimate. The flowchart of the data fusion algorithm in this paper is shown in Fig. 1.

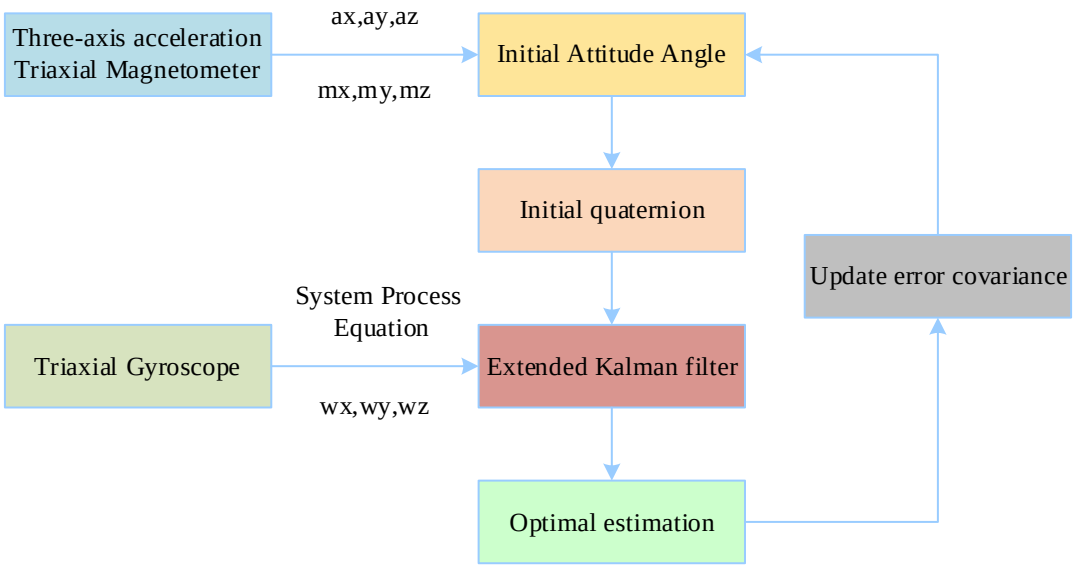

Figure 1. Flow chart of the proposed data fusion algorithm

In this paper, two coordinate systems are selected as the methods for attitude display. The geographic coordinate system and carrier coordinate system are selected as the inertial coordinate system. The rotation mode is defined as Z-Y-X, and its initial rotation quaternion is defined as $q(q_0, q_1, q_2, q_3)$. The data read by the nine-axis inertial sensor MPU9250 will generate cumulative errors, so we use the mean filtering method to preprocess the newly read data to eliminate the cumulative errors.

Define the initial pitch angle as:

$$\varphi = \arcsin\left(\frac{g_x}{g}\right) \tag{15}$$

The initial tumble angle is:

$$\theta = \arctan\left(\frac{g_x}{g_y}\right) \tag{16}$$

The initial heading angle is:

$$\psi = \arctan\left(\frac{m_y \cos\theta - m_x \sin\theta}{m_x \cos\varphi + m_y \sin\varphi \sin\theta + m_z \sin\varphi \cos\theta}\right) \tag{17}$$

The initial quaternion is obtained by converting the Euler angles to quaternions according to Eq. (18):

$$\begin{cases} q_0 = \cos\dfrac{\varphi}{2}\cos\dfrac{\theta}{2}\cos\dfrac{\psi}{2} + \sin\dfrac{\varphi}{2}\sin\dfrac{\theta}{2}\sin\dfrac{\psi}{2} \\ q_1 = \sin\dfrac{\varphi}{2}\cos\dfrac{\theta}{2}\cos\dfrac{\psi}{2} - \cos\dfrac{\varphi}{2}\sin\dfrac{\theta}{2}\sin\dfrac{\psi}{2} \\ q_2 = \cos\dfrac{\varphi}{2}\sin\dfrac{\theta}{2}\cos\dfrac{\psi}{2} + \sin\dfrac{\varphi}{2}\cos\dfrac{\theta}{2}\sin\dfrac{\psi}{2} \\ q_3 = \cos\dfrac{\varphi}{2}\cos\dfrac{\theta}{2}\sin\dfrac{\psi}{2} + \sin\dfrac{\varphi}{2}\sin\dfrac{\theta}{2}\cos\dfrac{\psi}{2} \end{cases} \tag{18}$$

The gyroscope establishes the state space equations of the system, and the data obtained from the gyroscope measurements can update the quaternions of the system, which can be obtained based on the attitude update theory in the inertial navigation system:

$$\begin{cases} \dfrac{dq}{dt} = \dfrac{1}{2}\omega_{ns}^{s} \otimes q \\ q_{k+1} = \exp\left(\omega\Delta t\right)^{*} q_k \end{cases} \tag{19}$$

Thus, the state space parameters of the system can be derived:

$$A_t = \begin{bmatrix} 1 & -\omega_x\dfrac{\Delta t}{2} & -\omega_y\dfrac{\Delta t}{2} & -\omega_z\dfrac{\Delta t}{2} \\ \omega_x\dfrac{\Delta t}{2} & 1 & \omega_z\dfrac{\Delta t}{2} & -\omega_y\dfrac{\Delta t}{2} \\ \omega_y\dfrac{\Delta t}{2} & -\omega_z\dfrac{\Delta t}{2} & 1 & \omega_x\dfrac{\Delta t}{2} \\ \omega_z\dfrac{\Delta t}{2} & \omega_y\dfrac{\Delta t}{2} & -\omega_x\dfrac{\Delta t}{2} & 1 \end{bmatrix} \tag{20}$$

The observation vectors of the system are established by means of accelerometers and magnetometers:

$$f = c_a^b \begin{bmatrix} 0 \\ 1 \\ 0 \end{bmatrix} = \begin{bmatrix} 2q_1q_2 + 2q_0q_3 \\ q_0^2 - q_1^2 - q_2^2 - q_3^2 \\ 2q_2q_3 - 2q_0q_1 \end{bmatrix} \tag{21}$$

Calculate the observation matrix of the system:

$$H = \frac{\partial f}{\partial q} = \begin{bmatrix} 2q_3 & 2q_2 & 2q_1 & 2q_0 \\ 2q_0 & -2q_1 & -2q_2 & -2q_3 \\ -2q_1 & -2q_0 & 2q_3 & 2q_2 \end{bmatrix} \tag{22}$$

The initial quaternion and the above parameters are brought into the extended Kalman filtering algorithm, and the final quaternion is calculated:

$$\begin{cases} \varphi = \mathrm{tg}^{-1}\dfrac{2\left(q_1q_2+q_0q_3\right)}{1-2\left(q_2^2+q_3^2\right)}, \varphi \in \left(0°, 360°\right) \\ \theta = -\sin^{-1}2\left(q_1q_3-q_0q_2\right), \theta \in \left(-90°, 90°\right) \\ \psi = \mathrm{tg}^{-1}\dfrac{2\left(q_2q_3+q_0q_1\right)}{1-2\left(q_1^2+q_2^2\right)}, \psi \in \left(0°, 360°\right) \end{cases} \tag{23}$$

The quaternions are converted to Euler angles according to Eq. (23) to be recorded as the attitude angles of their kinematic systems. Finally, these processed attitude angles are transmitted to the host computer for display.

2.3 Modeling the joints of rope skipping

After the data fusion algorithm completes the processing of the posture angle, it is necessary to restore the posture angle to the human body motion model, so it is essential to carry out the joint model design. The hardware device designed in this paper is worn to the back of the hand at a distance of about 3cm from the wrist joints, and the movement of the wrist joints can be measured through the movement of the hand motion posture information. When the wrist is placed horizontally to indicate its initial moment, the geographic coordinate system is noted as $O-XYZ$, the human body coordinate system at the wrist joint is displayed as $O_1-X_aY_aZ_a$, the hardware device is used as a carrier. The carrier coordinate system is noted as $O_b-X_bY_bZ_b$. The joint model design is shown in Figure 2.

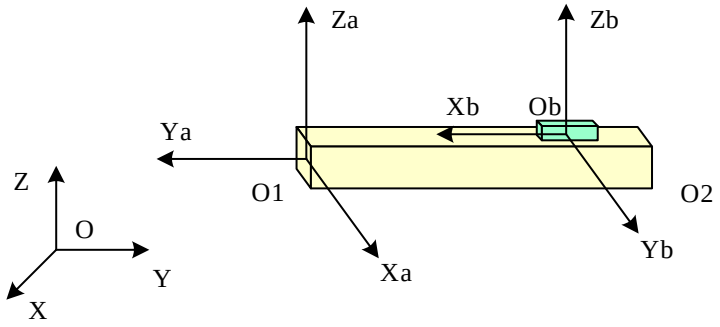

Figure 2. Joint model design

When the system is in the initial state, q_a is noted as the number of quaternions represented by the human body coordinate system and q_b represents the number of quaternions obtained by the carrier coordinate system through data acquisition and data processing:

$$q_{a0} = q_{b0} \otimes q_s \tag{24}$$

Equation (24), q_{a0} represents the quadratic value of the human body coordinate system at the initial moment, which is usually noted as $\left(\frac{\sqrt{2}}{2}, \frac{\sqrt{2}}{2}, 0, 0\right)$, q_{b0} represents the quadratic value of the carrier coordinate system at the initial moment obtained by measurement, and q_s represents the quadratic

number of the initial deviation between the carrier coordinate system and the geographic coordinate system. The initial deviation quaternion can be calculated from equation (22):

$$q_{a1} = q_{b1} \otimes q_s \tag{25}$$

When the joints start to move, q_{a1} represents the quadratic value of the human body at the joints during the movement, and q_{b1} represents the quadratic value of the current moment obtained by the sensor measurement, and the quadratic value of the human body at the joints at the current moment can be found out by Eq. (25).

From Fig. 2, it can be seen that the origin $O1$ remains unchanged when the movement of the wrist occurs, so the length of the hand can be measured as $l_{O1\vec{O}2}$. Therefore, the coordinates of the point $O2$ can be expressed as $(0,0,l_{O1O2})$, and the vector $O1\vec{O}2$ is denoted as $(0,0,0,l_{O1O2})$ using the quaternion method:

$$O1\vec{O}2' = q_{a1} \otimes O1\vec{O}2 \otimes q_{a1}^{-1} \tag{26}$$

From Eq. (26), the coordinates in the space of the final geographic coordinate system are obtained by calculating the vector $O1\vec{O}2$ with the quaternion q_{a1}, so that the angle between the wrist movement and the $O1O2$-axis is:

$$\partial = \arctan 2\left(2\left(q_0 q_3 + q_1 q_2\right), 1 - 2\left(\left(q_2\right)^2 + \left(q_3\right)^2\right)\right) \tag{27}$$

The q_0, q_1, q_2, q_3 in Eq. (27) denotes the quaternion at q_{a1}, from which the human body's jumping rope movement posture can be restored by the posture angle.

3 Wearable jump rope motion capture system design

3.1 General program design of the system

The main functions of the wearable rope skipping motion capture system designed in this paper include data acquisition and processing, data transmission, and calculation and rendering of human whole body posture. The sensor and processor mainly do the data acquisition and calculation, the WI-FI module mainly does the data transmission, and the calculation and animation rendering of the whole body posture is realized primarily by the PC and animation rendering software.

In order to capture the jumping rope movement, it is necessary to place the data acquisition module in the key position of the target's whole body. The data acquisition module needs to collect the human body jumping rope movement information data calculate the three-dimensional spatial posture, and then send the data to the display rendering program of the computer through wireless transmission to drive the three-dimensional model movement. Since the position of the node sensors on the human body cannot be fixed every time, it is necessary to calibrate the multi-node sensors together before use. The requirements analysis dictates that the paper's design must meet the following points:

1) Hardware part: 15 sensor nodes consisting of MEMS sensors and WI-FI modules, a router, and a computer.

2) Software part: single-node 3D spatial posture calculation algorithm based on accelerometer, gyroscope, and magnetometer, hierarchical 3D model of the human body, and multi-node posture fusion algorithm of the human body.

In summary, the ultimate purpose of this paper is to design and fabricate a motion-tracking system that can track the effects of jumping rope movements. The system is mainly composed of a data acquisition module and a human body model attitude reconstruction part, in which the data acquisition module is primarily responsible for collecting data, solving the spatial 3D attitude of a single node, and transmitting the data to the host computer, which receives the data of each node, adds constraints, and fuses the data of all nodes' postures to compute the whole body attitude data of the human body, which is synchronized to the 3D model. The system's overall structural design can be seen in Figure 3.

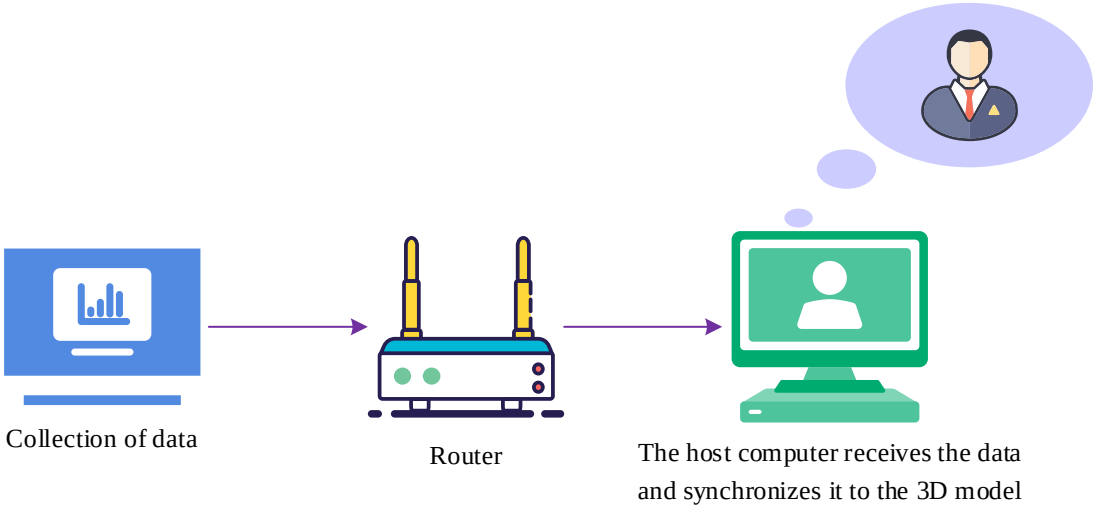

Figure 3. General architecture block diagram of the system

3.2 Hardware Acquisition Node Design

3.2.1 System Hardware Program Design

In order to realize the capture and tracking of human jumping rope movement, it is necessary to bind the posture measurement equipment to the middle of each important skeletal segment of the human body, real-time acquisition of the movement parameters of the human body during the jumping rope movement, and then substitute the acquired parameters into the data fusion and posture solving algorithm, in order to calculate the jumping rope movement of the human virtual model.

The data acquisition module needs to fulfill three functions: data acquisition, attitude solving, and data transmission. The node unit will collect real-time jumping rope movement attitude data at a fixed frequency, calculate the attitude information of the current single node according to the data, and transmit the attitude data to the host computer in real-time through wireless transmission. The hardware acquisition system's framework is depicted in Fig. 4.

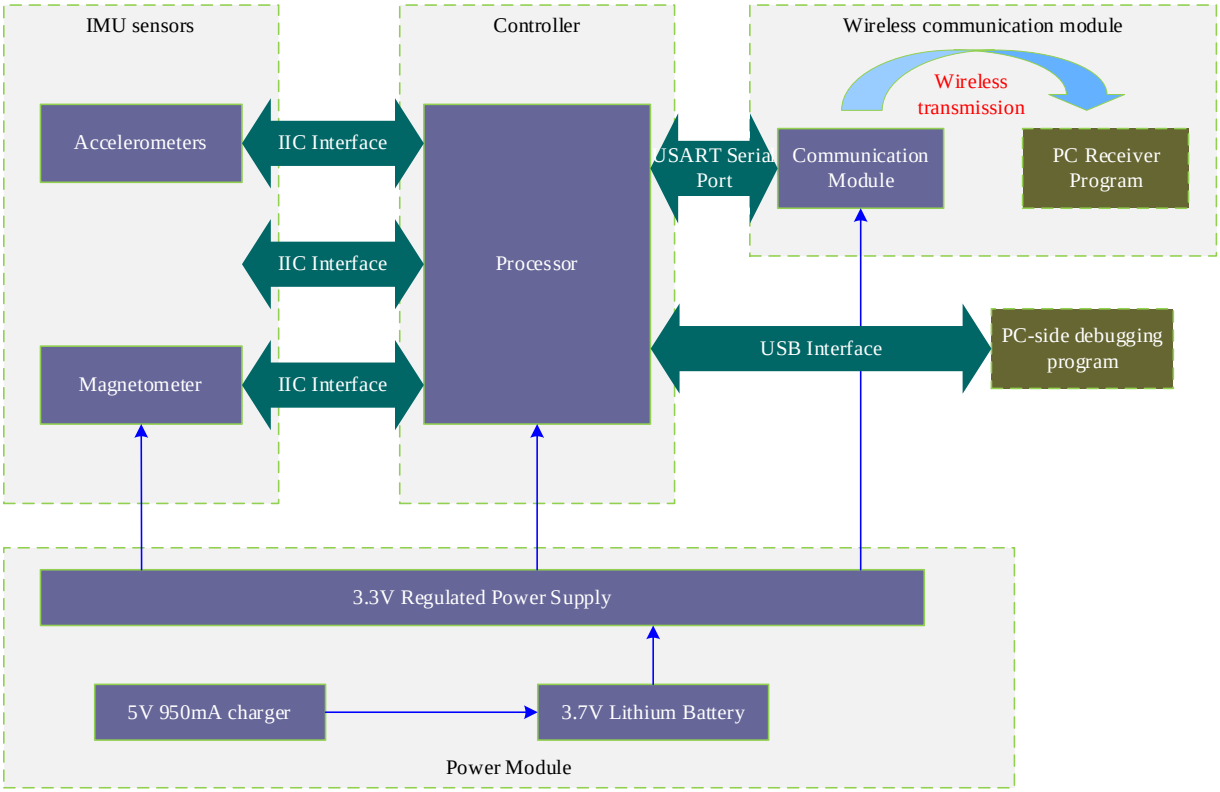

Figure 4. Frame diagram of the hardware acquisition system

3.2.2 Sensor selection

The inertial sensor unit is the data acquisition module for each node of the human body, which is mainly composed of a power module, a data acquisition module, and a wireless communication module. Its main role is to continuously collect motion data information of the carrier through the sensors, calculate the 3D attitude angle of individual nodes, and send it to the host computer for processing.

With the continuous deep research of sensor technology and the rapid and stable development of the manufacturing process, the current market has a variety of models of inertial sensors for us to choose from, with different sizes, accuracy, and other parameters. Not only are there separate gyroscopes, accelerometers, and magnetometers. There are also a variety of sensors combined in a module, such as MPU6050, MPU9250, and so on. The composition module has two kinds of six-axis sensor and nine-axis sensor, of which the nine-axis sensor has more magnetometer than the six-axis sensor. In attitude angle solving, compared with the nine-axis sensor six-axis sensor solving algorithm is relatively simpler. The calculation amount is small, but there is the phenomenon of heading angle drift, which will greatly affect the accuracy of the long-time use.

According to the requirements of this paper, several sensor units are designed and fabricated to be placed at the head, back, waist, left and right upper arms, and left and right lower arms. Right hands, left and right thighs, left and right calves, and left and right feet, respectively. In this paper, the nine-axis sensor module MPU9250 is chosen as the data acquisition sensor of the node.MPU9250 consists of two parts, one of which is the accelerometer and gyroscope chip integrated, and the other one is the three-axis magnetic intensity sensor. Compared with other nine-axis sensors, MPU9250 has the advantages of small size and light weight, which fully meets the accuracy requirements of this system.

Moreover, MPU9250 comes with an IIC transmission interface, and the sampling rate of the sensor meets the usage requirements. The module package can be seen in Figure 5.

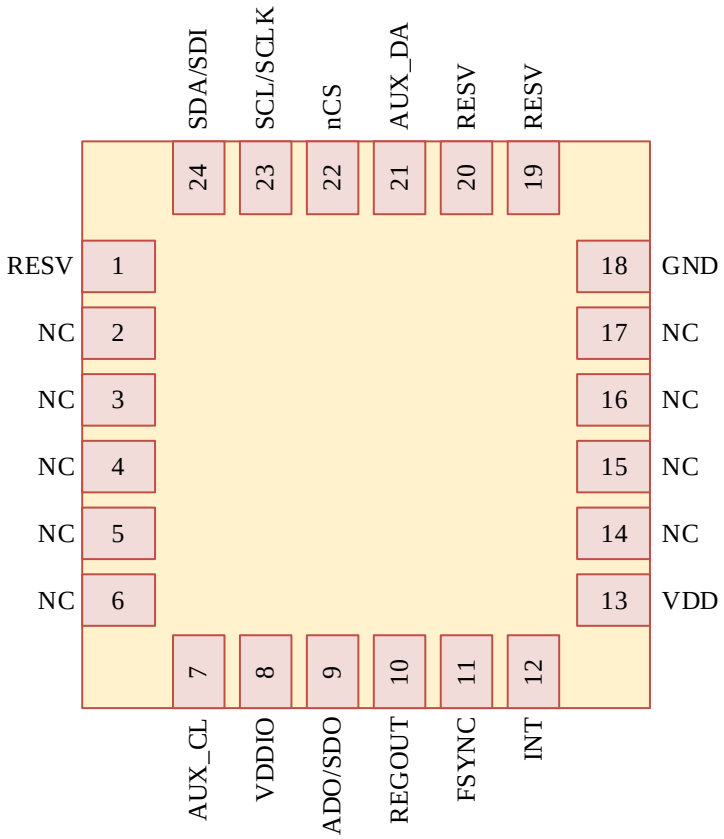

Figure 5. MPU9250 module packaging diagram

3.2.3 Sensor Node Software Design

The main function of the sensor node is to read and analyze real-time attitude data and solve the current azimuth information of the sensor. The software part of the sensor node consists of two main parts: the first part is the data reading, processing, and sending program based on the Arduino development environment, and the second part is the Arduino IDE, the program development environment in the computer.

The sensor uses JSON format to send data. JSON (JavaScript Object Notation) is a new type of text exchange format, which adopts a text format completely independent of the programming language, which is easy for people to use and understand, as well as easy for the program to be parsed and produced, so it is widely used. Figure 6 displays the software flowchart for the sensor node.

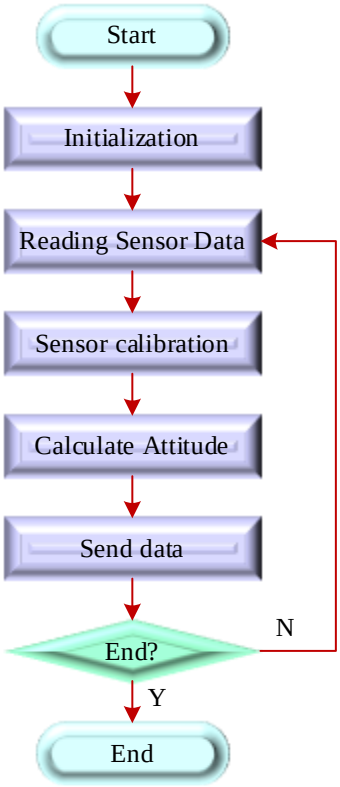

Figure 6. Software flowchart of sensor nodes

4 Experimental analysis of the tracking effect of rope skipping

4.1 Single Node Attitude Test

4.1.1 Static tests

The sensor is fixed on a bracket, controlled around another bracket parked at different angles through the static, fixed attitude comparison of the solved attitude information and the real rotation angle. In order to assess the performance of the fixed attitude solving accuracy, the experiments randomly selected a few fixed rotation angles, and each angle experiments 30 times to take the average value of the statistics. The statistical results are shown in Table 1.

From Table 1, it can be seen that by comparing the fixed rotation angle and the sensor pose-solving angle, the error is controlled within 1.4°, and the result of data solving is basically correct, which can output the pose information of the jump rope node well.

Table 1. Statistical results

True Angle of rotation/°	Angle of resolution/°	Deviation/°
25	26.4	1.4
40	39.3	-0.7
55	55.5	0.5
70	71.3	1.3

4.1.2 Dynamic testing

By transforming the placement direction of the sensor and controlling the running speed of the motor, the full attitude information of the simulated joint motion is achieved by controlling the rotation of the bracket. The motor rotation speed is controlled between 20°/s and 270°/s, and the range of rotation is from 0° to 90°, and the controlled rotation speed of the motor and the solved information of the sensor are compared. The dynamic angle comparison results are shown in Fig. 7.

From Fig. 7, it can be seen that in the motion state, the dynamic accuracy of the solving based on the attitude information of the inertial sensor is about 4°. The direction of the solving curve and the real curve are basically the same as that of the real curve on the whole, so the inertial sensor responsiveness is the same as the actual action. However, when the action speed changes drastically, the solving result will have a small fluctuation, which is due to the inconsistency of each sensor node when working together, leading to the misjudgment of the wrong data in the data transmission judgment.

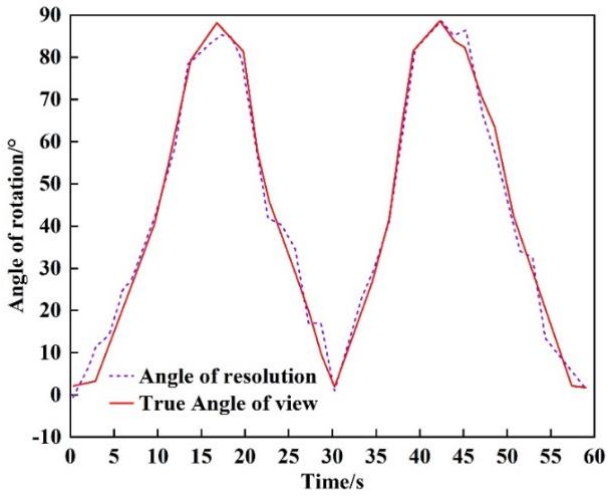

Figure 7. Comparison of dynamic angle

4.2 Comparative Experiments on Jump Rope Posture Solving

Design the human right-hand motion experiment by aligning and stacking the sensor nodes of this paper with the coordinate system of commercial nine-axis motion sensors for jumping rope motion and comparing the attitude solution results of this paper based on the data fusion algorithm and D-H method with the attitude solution results realized by the nine-axis motion sensor device. The test results for attitude solving are shown in Fig. 8, (a) ~ (c) are the pitch angle, flip angle, and yaw angle, respectively.

From (a) graph in Fig. 8, it can be seen that the pitch angle solved in this paper deviates slightly from the commercial nine-axis sensor when the number of sample points is at [31,66], while the other parts are basically consistent. From (b) figure, when the number of sample points is [168,174], the flip angle solved in this paper is slightly smaller than that of the commercial nine-axis sensor, while the other parts are almost completely coincident. From the (c) figure, it can be seen that the deviation of the yaw angle curve between this paper's solution and the commercial nine-axis sensor is slightly larger than that of the pitch angle and the flip angle. Still, the curve direction is basically the same, and the deviation is small. The performance of the algorithm in this paper is very similar to the attitude solution of the commercial nine-axis motion sensor.

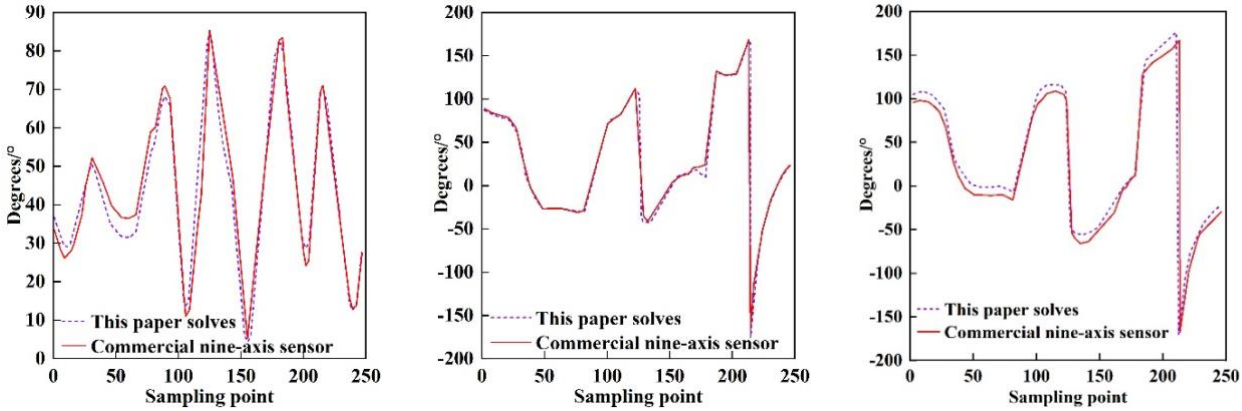

(a) Angle of pitch (b) Angle of roll (c) Angle of yaw

Figure 8. The test results of attitude solving

Taking the real reference values of the attitude values solved by the commercial nine-axis motion sensors, the root mean square error (RMSE) values of the three attitude angles for the attitude solving of the data fusion algorithm of this paper are calculated, where the RMSE values are computed as in equation (28):

$$RMSE = \sqrt{\frac{\sum_{i=1}^{n}\left(X_{solved} - X_{ref}\right)^2}{n}} \tag{28}$$

Where n is the number of sampling points, X_{solved} is the attitude angle value solved by the data fusion algorithm in this paper, and X_{ref} is the attitude angle value measured by the corresponding commercial nine-axis motion sensor. The results of the root mean square error values for the three attitude angle values are shown in Table 2.

As can be seen from Table 2, the RMSE values of pitch angle, roll angle, and yaw angle range from [0.24,0.46], [0.26,0.92], and [1.17,1.66], respectively, and the average values of RMSE are 0.37, 0.71, and 1.40, respectively. The values of RMSE are all small, which indicates that the attitude-solving results of this paper's algorithms are very close to the solving results of the commercial nine-axis motion sensors. Thus, it shows that the wearable device used in this paper and the attitude-solving algorithm based on the data fusion algorithm and the D-H method can reach the standard of commercial nine-axis motion sensors, and real-time tracking of jumping rope movement can be carried out.

Table 2. Table of RMSE values of attitude angles

Number of experiments	1	2	3	4	5	6	7
Angle of pitch	0.35	0.24	0.43	0.46	0.38	0.38	0.34
Angle of roll	0.82	0.75	0.92	0.26	0.78	0.71	0.70
Angle of yaw	1.29	1.25	1.56	1.27	1.17	1.57	1.66

5 Conclusion

The design of a wearable rope-skipping motion capture system is based on the acquisition, processing, transmission, calculation, and animation rendering of human whole body posture. The sensor and the processor mainly do the data acquisition and calculation, the WI-FI module mainly does the data transmission, and the calculation and animation rendering of the human body's whole-body posture are realized primarily by the PC and the animation rendering software. The hardware part of the system includes sensor nodes composed of MEMS sensors and WI-FI modules, a router, and a PC. In contrast, the software part consists of a single-node 3D spatial posture calculation algorithm, a hierarchical 3D model of the human body, and a multi-node posture fusion algorithm of the human body. The focus of this paper is on the experimental analysis of the sensors used and the pose-solving algorithm.

The experimental results of the single-node attitude test show that the static test error of the sensor is controlled within 1.4°, and the results of data solving are basically correct, which can output the attitude information of the node well. The inertial sensor's attitude information in the motion state is 4° dynamically accurate, and responsiveness is basically consistent with the actual action. The sensor nodes will be inconsistent when working together when the jumping rope action changes drastically, leading to incorrect data transmission judgments.

In addition, in order to verify its commercial value, the comparison test with the commercial nine-axis motion sensor shows that the yaw angle curve deviation is slightly larger than the pitch and roll angles. Still, the curve direction is basically the same, and the deviation is small. The RMSE of pitch angle, roll angle, and yaw angle take values in the ranges of [0.24,0.46], [0.26,0.92] and [1.17,1.66], respectively, and the average values of the RMSE are 0.37, 0.69, and 1.40, respectively. It can be seen that the wearable device and the attitude-solving algorithms used in this paper are able to meet the standard of commercial application.

References

[1] Rapp, A., & Tirabeni, L. (2018). Personal informatics for sport. ACM Transactions on Computer-Human Interaction (TOCHI).

[2] Mcdonough, D. J., Su, X., & Gao, Z. (2021). Health wearable devices for weight and bmi reduction in individuals with overweight/obesity and chronic comorbidities: systematic review and network meta-analysis. British Journal of Sports Medicine, 55(16), 1-11.

[3] Yeung, K. K., Huang, T., Hua, Y., Zhang, K., & Gao, Z. (2021). Recent advances in electrochemical sensors for wearable sweat monitoring: a review. IEEE Sensors Journal, PP(99), 1-1.

[4] Chon, T. J., Sung, D. J., Jeon, J. Y., & Shin, J. T. (2018). Enhancing psychological and physical fitness factors of korea middle school students by introducing rope skipping. Iranian Journal of Public Health, 47(12), 1965-1966.

[5] Wu, J., & Jafari, R. (2017). Seamless vision-assisted placement calibration for wearable inertial sensors. Acm Transactions on Embedded Computing Systems, 16(3), 1-22.

[6] T, Alt, Y, T, Nodler, & J, et al. (2017). Velocity-specific and time-dependent adaptations following a standardized nordic hamstring exercise training. Scandinavian journal of medicine & science in sports.

[7] A, J. R., A, N. L., A, Z. Z., A, J. S., A, L. L., & B, L. X., et al. (2018). All-fiber-based quasi-solid-state lithium-ion battery towards wearable electronic devices with outstanding flexibility and self-healing ability. Nano Energy, 51, 425-433.

[8] Sung, K. D., Pekas, E. J., Scott, S. D., Son, W. M., & Park, S. Y. (2020). The effects of a 12-week jump rope exercise program on abdominal adiposity, vasoactive substances, inflammation, and vascular

function in adolescent girls with prehypertension (vol 119, pg 577, 2019). European journal of applied physiology(5), 120.

[9] Jiang, Q., Qian, Y., Ma, J., Ma, X., Cheng, Q., & Wei, F. (2019). User centric three-factor authentication protocol for cloud-assisted wearable devices. International Journal of Communication Systems, 32(6), e3900.1-e3900.20.

[10] Guo, W. (2018). Brain science and physical education-to promote harmonious development of students with combination of left and right brain in physical education. NeuroQuantology, 16(5).

[11] Ha, A. S., Ng, J. Y. Y., & Mary, S. C. (2017). Rope skipping increases bone mineral density at calcanei of pubertal girls in hong kong: a quasi-experimental investigation. Plos One, 12(12), e0189085.

[12] David Hortigüela Alcalá, Fonseca, A. J. S., & Hernandez-Elizondo, J. (2018). Original motivational contrast in physical education depending on caloric expenditure contraste motivacional en educacin fsica en funcin del gasto calrico. Revista Internacional de Medicina y Ciencias de la Actividad Fisica y del Deporte, 18(72), 621-635.

[13] Johnston, W., Judice, P. B., Pablo Molina García, Jan M Mühlen, & Sardinha, L. B. (2020). Recommendations for determining the validity of consumer wearable and smartphone step count: expert statement and checklist of the interlive network. British Journal of Sports Medicine.

[14] Huang, Y., Hu, M., Muthu, B. A., & Gayathri, R. (2021). Wearable energy efficient fitness tracker for sports person health monitoring application. Journal of Intelligent and Fuzzy Systems(5), 1-10.

[15] Sattler, M. C., Ainsworth, B. E., Andersen, L. B., Foster, C., & Poppel, M. N. M. V. (2021). Physical activity self-reports: past or future?. British Journal of Sports Medicine, bjsports-2020-103595.

[16] Dargazany, A. R., Stegagno, P., & Mankodiya, K. (2018). Wearabledl: wearable internet-of-things and deep learning for big data analytics—concept, literature, and future. Mobile Information Systems, 2018, 1-20.

[17] Wang, Y., & Gong, X. (2021). Optimization of data processing system for exercise and fitness process based on internet of things. Wireless Communications and Mobile Computing.

About the Author

Diyang Liu (1990-), Male, Han, Weifang, Shandong, teaching assistant, PhD, research direction: exercise training, synchronized jump rope.

Qiang Zhang (1990-), Male, Han, Fuyang, Anhui, lecturer, PhD, research direction: sports education training.